

1 **Effects of the Three Gorges Dam Operation on the**
2 **hydrological interaction between the Yangtze River and**
3 **downstream aquifers**

4
5 Qi Zhu¹, Ye Kang¹, Zhang Wen^{1*}, Hui Liu¹, Luguang Liu², Yan Li², Xu Li³, Eungyu
6 Park⁴

7
8 1. ¹Hubei Key Laboratory of Yangtze Catchment Environmental Aquatic Science,
9 School of Environmental Studies, China University of Geosciences, Wuhan 430074,
10 Hubei, People's Republic of China

11 2. Hubei Water Resources Research Institute, Wuhan 430070, People's Republic of
12 China

13 3. School of Earth and Environment, Anhui University of Science and Technology,
14 Huainan, People's Republic of China

15 4. Department of Geology, Kyungpook National University, Daegu, Republic of
16 Korea

17

18

19 *Correspondence to:* Zhang Wen (wenz@cug.edu.cn)

20 **Abstract.** The construction of the Three Gorges Dam (TGD) has profoundly altered
21 the groundwater cycle downstream. The obscure spatiotemporal patterns of exchange
22 fluxes between the Yangtze River and groundwater hinder the resolution of water
23 resources and environmental issues in the watershed. In the Four-Lake Basin, the first
24 river-lake wetland plain downstream of the TGD, this study investigated the spatial
25 extent of the Yangtze River's influence on adjacent groundwater by leveraging
26 multiple groups of monitoring wells installed along the river. A coupled SWAT-
27 MODFLOW model was applied to quantify period-specific surface water-
28 groundwater exchanges. A counterfactual scenario without TGD operation-holding
29 other conditions constant is also simulated for comparison. The results show: (1)
30 Under the combined influence of hydrogeological conditions and distance from the
31 TGD, the influence range of the Yangtze River on confined groundwater is
32 significantly greater in the upper section than in the lower section of the Four-Lake
33 Basin, with a difference of approximately one order of magnitude. (2) River and
34 groundwater exchanges exhibit pronounced seasonal and spatial characteristics: river-
35 to-aquifer recharge dominates during drawdown and flooding periods, while aquifer-
36 to-river discharge dominates during impounding and dry periods. Using JLX2 as a
37 divider, interaction rates are consistently higher in the upper section than in the lower
38 one. (3) Relative to natural conditions, TGD operation dramatically dampens Yangtze
39 River-groundwater interactions overall. The effect is most pronounced during the dry
40 period in the upper section, when the interaction rate decreases by 40.6%. These
41 research outcomes serve as a vital theoretical foundation for assessing the effects of
42 the TGD's regulation on the regional water cycle.

删除[Zhu Qi]: The influence range of the Yangtze River on confined groundwater is larger in the ZJ-JLX2 section (upper section below the TGD), whereas it is relatively minor on groundwater near HH1 profile and HH2 profile (lower section below the TGD). The influence distance at the HH1 profile is the smallest, measuring as 1.94 km.

43 **1 Introduction**

44 High-dam reservoirs play a critical role in flood mitigation, hydroelectric power
45 generation, water supply, and navigation (Poff et al., 1999). To date, approximately
46 50% of rivers worldwide are regulated by dams (Van Cappellen et al., 2016). The
47 dam's impact on the riparian hydrology and biogeochemistry is so pronounced
48 (Palmer and Ruhi, 2019; Song et al., 2020; Maavara et al., 2020) that it can even
49 surpass the effects of hydrological extremes (Dewey et al., 2022). The Three Gorges
50 Dam (TGD), a mega-engineering structure on the mainstream of the Yangtze River,
51 functioned as a "master valve" controlling flow in the middle reaches. Operational
52 strategies such as "storing water in early autumn" and "releasing water in winter and
53 spring" have substantially altered the river's natural hydrological regime (Wang et al.,
54 2016; Guo et al., 2022).

55 Centrally located in the Middle Yangtze Basin, the Four-Lake Basin is the first
56 large river-lake wetland system downstream of the TGD. It supports an integrated
57 ecosystem of rivers, lakes, reservoirs, and farmlands (Zhang et al., 2023) and plays a
58 vital role in flood regulation, ecological stabilization, and sustaining agricultural
59 economies (Zhou et al., 2013). However, since the TGD became operational, nitrogen
60 and phosphorus pollution in the water bodies of the middle Yangtze River basin,
61 particularly in areas such as the Four-Lake Basin, has intensified (Gao et al., 2021; Hu
62 et al., 2023; Zhou et al., 2023). While extensive research has documented the impacts
63 of the TGD on the regional water cycle (e.g., Deng et al., 2016; Xiong et al., 2020;
64 Wu et al., 2023), the precise quantification of how TGD-induced river stage
65 fluctuations affect groundwater levels and river-aquifer exchange fluxes, particularly
66 at the basin scale, remains a critical and ongoing challenge.

67 Unlike surface-water-dominated systems, many lakes, rivers, and agricultural
68 wetlands in the Four-Lake Basin interact with the Yangtze mainly through subsurface

69 groundwater exchange (Deng et al., 2016). Yet the extent of the Yangtze's influence,
70 which is a key driver of regional hydrological and ecological processes (Hu et al.,
71 2023; Lai et al., 2025), remains poorly quantified, hindering a clear understanding of
72 groundwater cycling and its ecological consequences. Moreover, TGD operations
73 have introduced significant spatiotemporal variations in water levels along the
74 Yangtze mainstream. Combined with the high spatial heterogeneity of
75 hydrogeological conditions in the riparian zone, these changes complicate efforts to
76 characterize river-groundwater interactions. Although prior research has illuminated
77 local-scale exchange processes (Wang & Wörman, 2019; Huang et al., 2023), such
78 insights are insufficient for assessing basin-wide impacts, underscoring the need for
79 broader monitoring and systematic investigation.

80 Since the TGD's completion, its effects on various downstream ecological
81 components, such as lake levels (Huang et al., 2021), wetland evolution (Zhang et al.,
82 2012), sediment transport (Yang et al., 2007), channel morphology (Sun et al., 2012;
83 Yang et al., 2014), and eco-hydrological conditions affecting vegetation (Xie et al.,
84 2014), have attracted considerable research attention. Nevertheless, the dam's impacts
85 on groundwater systems remains inadequately understood, especially in terms of
86 quantitative attribution isolated from other influencing factors. In the Four-Lake Basin,
87 the presence of an intricate flood-control network further complicates the study of
88 water interactions (World Bank, 2023).

89 While previous quantitative studies have examined hyporheic exchange in the
90 Jiangnan Plain (Du et al., 2018; Jiang et al., 2022), they do not fully account for the
91 compounded effects of hydroclimate, TGD operations, spatial heterogeneity in
92 hydrogeological conditions, and local flood-control and irrigation infrastructure on
93 Yangtze-groundwater interactions in the Four-Lake Basin. To be more precise, in
94 addition to being influenced by the Yangtze River, groundwater levels along the river

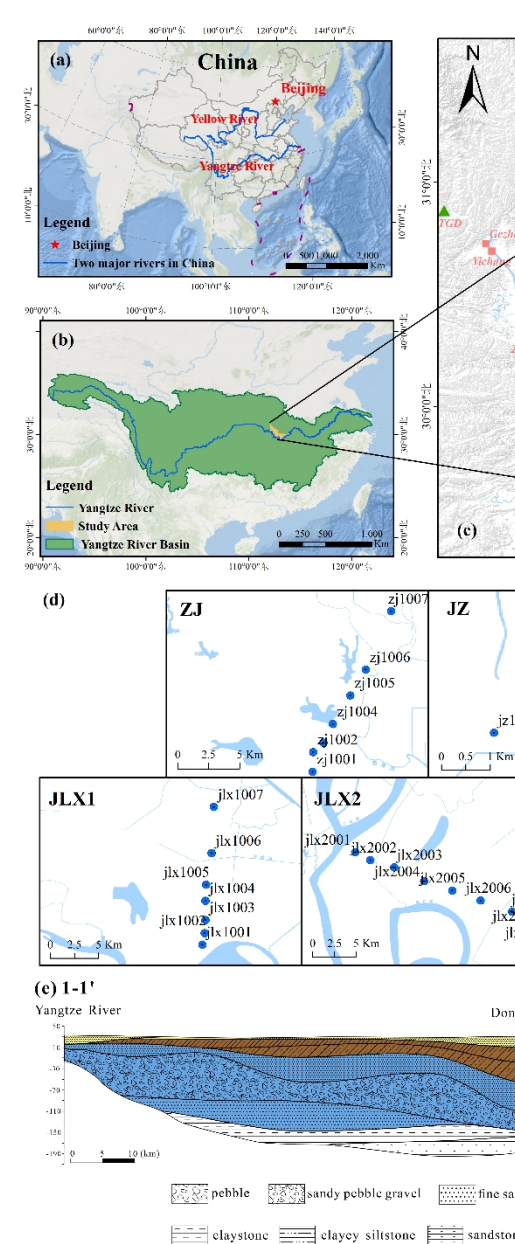
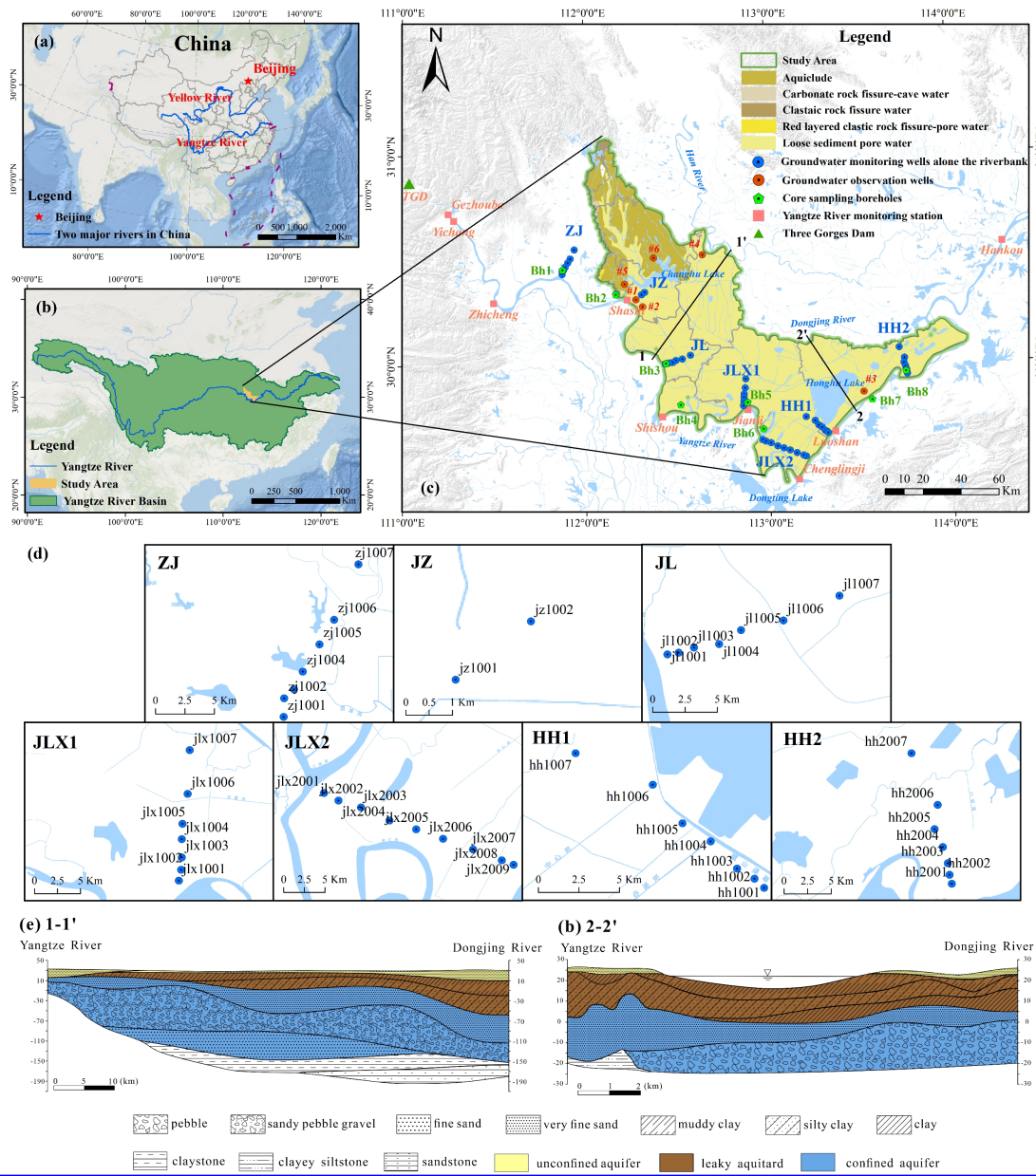
95 are often affected by factors such as runoff generation and concentration, surface soil
96 water infiltration, and recharge from the local surface water network. These factors
97 make traditional groundwater numerical modeling approaches struggle to accurately
98 capture fluctuations in the groundwater table, thereby introducing significant errors in
99 characterizing the exchange processes between the Yangtze River and groundwater.

100 To address these complexities, the SWAT-MODFLOW model offers a robust
101 physically-based framework. This coupled model has been extensively utilized
102 worldwide to simulate complex regional surface water-groundwater (SW-GW)
103 interactions, such as evaluating the effects of agricultural irrigation in the United
104 States (Aliyari et al., 2019), assessing how climate and land-use changes impact
105 groundwater quality in European river basins (Pulido-Velazquez et al., 2015), and
106 analyzing nutrient transport in large river basins in China (Yang et al., 2024).
107 Obviously, for the Sihu Basin which is distributed with numerous wetlands and water
108 bodies such as rivers, lakes, and paddy fields along the Yangtze River, SWAT-
109 MODFLOW demonstrates high feasibility in characterizing how the groundwater
110 flow system within its complex Quaternary sedimentary formations is influenced by
111 surface terminal water bodies under the regulation of the Three Gorges Reservoir.

112 Aiming to bridge these gaps, this study focuses on the interplay between the
113 Yangtze River and groundwater in the Four-Lake Basin. Data from seven monitoring
114 profiles will be used to demarcate the spatial influence of the Yangtze River on
115 aquifer dynamics. Based on this influence range, the impact of surface water bodies
116 on groundwater is clearly defined, thereby guiding the development of a field-
117 calibrated SWAT-MODFLOW model to analyze the effects of TGD operations on
118 SW-GW interactions. Ultimately, by constructing a counterfactual scenario without
119 the dam, we aim to isolate and quantify the specific impact of the TGD, providing a
120 quantitative assessment of its influence.

121 **2 Overview of the Study Area**

122 Situated downstream of the TGD on the middle Yangtze's northern bank, the
123 Four-Lake Basin covers an area of about 11,547 km² (Fig. 1). Its boundaries are
124 formed by a combination of natural and artificial features. To the northwest lie the
125 hills of Jingmen and Jiangling counties along with the Zhang River irrigation district;
126 to the north is the watershed of the Han River Basin; and to the east and south, it is
127 bordered by the Yangtze River. The basin's climate is characterized by a mean annual
128 temperature of 15~17 °C, with annual precipitation and evaporation averaging 1,269
129 mm and 1,200 mm, respectively. Located in a flat alluvial plain with an average
130 elevation of 27 m. the Four-Lake Basin features a dense network of interconnected
131 lakes, rivers, and canals, among which Honghu and Changhu Lakes are the most
132 prominent. The Four-Lake Main Channel, as the primary artery of the basin, connects
133 these major lakes and their tributaries, ultimately discharging into the Yangtze River.
134 Groundwater mainly receives combined recharge from precipitation and surface water.
135 Only in a small portion of the northwestern upland areas does groundwater recharge
136 occur predominantly from precipitation, followed by discharge toward the
137 surrounding low-lying plains (Lan et al., 2025; Li et al., 2023). The groundwater table
138 is generally shallow, typically lying 2~5 m below the surface, which facilitates
139 widespread groundwater utilization.



删除[k k]:

140

141 Figure 1: Map of the study area and monitoring network in the Four-Lake Basin, showing (a) the
 142 regional context of the Yangtze River (adapted from the basemap in Esri., 2023), (b) the basin location
 143 (adapted from the basemap in Esri., 2023), (c) surface water and groundwater monitoring stations in
 144 the map indicating different types of groundwater, which is entirely compiled according to the internal
 145 survey data from the author's institution, (d) groundwater monitoring wells installed along each profile,

146 (e) Stratigraphic profile 1-1' near Jiangling (JL) Profile, and (f) Stratigraphic profile 2-2' near Honghu
147 (HH) Profile.

148 The study area features a groundwater system composed of an unconfined
149 aquifer and multiple confined aquifers. The unconfined aquifer, primarily distributed
150 across the flat central and eastern basin, consists of silty clay, silt, and fine sand, with
151 localized thin gravel layers. Its thickness typically ranges from 3 to 10 m. The upper
152 confined aquifer, which is the most extensive in the region, is composed of clay, silty
153 clay, muddy silty clay, sand, and gravel. Its thickness exhibits considerable spatial
154 variation, generally increasing from the western and peripheral zones toward the
155 central and eastern parts of the basin. In contrast, the lower confined aquifer is
156 predominantly composed of gravel (Huang et al., 2023). Figures 1(e) and 1(f)
157 illustrate the geological cross-sections for profiles 1-1' and 2-2' (locations indicated
158 in Fig. 1c), respectively. From the upstream to the downstream of the basin, the
159 thickness of the clay confining layer increases significantly, while the lithology of the
160 underlying aquifer transitions from highly permeable gravel and pebbles to lower-
161 permeability fine sand.

162 **3 Data and Methods**

163 **3.1 Data Sources**

164 We established a network of groundwater monitoring profiles along the northern
165 bank of the Yangtze River within the Four-Lake Basin, comprising seven distinct
166 profiles-Zhijiang (ZJ), Jingzhou (JZ), Jiangling (JL), Jianli1 (JLX1), Jianli2 (JLX2),
167 Honghu1 (HH1), and Honghu2 (HH2)-with a total of 46 monitoring wells (Fig. 1).
168 Within each profile, wells were systematically positioned at distances of 1, 2, 3, 5, 7,
169 10, 15, 20, and 25 km from the landside toe of the Yangtze River embankment.
170 Groundwater levels were monitored from January 1 to December 31, 2021, at regular

171 5-day intervals. The year 2021 was chosen for investigation due to the availability of
 172 a comprehensive dataset from 46 monitoring wells. These wells, arranged in
 173 systematic profiles, provide high spatial density for analyzing lateral water signal
 174 propagation. Additionally, the 5-day monitoring interval is sufficient to capture the
 175 seasonal and operational fluctuations induced by the TGD.

176 The SWAT model primarily required two types of data: spatial data (including
 177 elevation, land use, and soil type data) and meteorological data, with the specific data
 178 formats and sources listed in Table 1. The MODFLOW model necessitated
 179 hydrogeological parameters, recharge and discharge components, and calibration data
 180 derived from long-term groundwater level observations.

181 Table 1 Data types and sources of SWAT model.

Data Type	Data Accuracy	Description	Sources
Digital Elevation Model (DEM)	30 m×30 m	ASTERG DEM V3	Geospatial Data Cloud Platform https://www.gscloud.cn/
Landuse Data	1km×1km	Distribution of land use types	Data Center for Resources and Environmental Sciences https://www.resdc.cn/
Soil Type Data	30m×30 m	Soil type and soil physical properties	Harmonized World Soil Database https://www.fao.org/
Meteorological Data	1/8°×1/8°	Daily average relative humidity, daily cumulative 24-hour precipitation, daily average solar radiation, daily maximum and minimum temperatures, and daily average wind speed	China Meteorological Assimilation Driving Datasets (CMADS V1.2) https://poles.tpc.ac.cn/

182 The calibration of the MODFLOW model utilized groundwater level data (2011-
 183 2013) obtained from a hydrogeological field investigation conducted in the Jiangnan
 184 Plain during this period (Wen et al., 2017), nearly a decade after the impoundment of
 185 the TGD. To maintain consistency, the same timeframe was adopted for the surface
 186 hydrological modeling data in SWAT to facilitate the model's validation.

187 **3.2 Research Methods**

188 3.2.1 Spatial response analysis of water-level

189 Given that the unconfined aquifer along the Yangtze River is subject to multiple
190 factors—including river stage, precipitation, surface water bodies, and human
191 activities—the water level exhibits frequent fluctuations. This study, therefore,
192 focuses on quantifying the lateral influence of the river on the more stable confined
193 aquifer along its north bank. To this end, water-level data from the confined aquifer
194 were collected through monitoring profiles to investigate the fluctuation patterns of
195 both the river stage and the confined groundwater, as well as the spatial extent of the
196 river's influence. The analytical procedure is detailed below:

197 (1) Data collection and analysis. The river stages and corresponding groundwater
198 levels from the seven monitoring profiles (ZJ, JJ, JL, JLX1, JLX2, HH1, and HH2)
199 with complete 2021 datasets were selected for analysis (Fig. 1). For each month, the
200 daily maximum water level of the Yangtze River was identified, and the
201 corresponding groundwater levels in monitoring wells at various distances were
202 recorded simultaneously. The differences between the maximum water levels of the
203 Yangtze River and groundwater in consecutive months were calculated to derive the
204 fluctuation amplitudes of both at a monthly interval. As shown in the subplot of the
205 ZJ profile in Fig. A1 in the Appendix A, the legend "1/9–2/17" indicates that January
206 9 and February 17 represent the days when the peak water levels of the Yangtze River
207 occurred in their respective months. The difference in water levels between these two
208 days forms the black polyline in the figure. It is important to note that the monthly
209 maximum water level of the Yangtze River was selected because the peak value is the
210 most prominent and objectively identifiable feature, avoiding subjectivity in selecting
211 dates during periods of mild fluctuation. Moreover, the high water level exerts the

212 strongest driving force on the adjacent groundwater, theoretically maximizing the
213 reflection of groundwater response to changes in the Yangtze River water level.

214 (2) Construction and fitting of water-level spatial response equations. A critical
215 step in this analysis was to develop empirical equations that quantify the response of
216 groundwater levels to fluctuations in the Yangtze River stage at different distances
217 from the river. Unlike previous studies, such as Wang and Wörman (2019), which
218 focused mainly on temporal variations in groundwater, the present study employs the
219 analytical solution proposed by Liu et al. (2021) to demonstrate the exponential
220 attenuation of groundwater response amplitudes with distance from the riverbank
221 under sinusoidal river-stage variations, which can be expressed as:

$$222 \quad y = a \cdot e^{bx} \quad (1)$$

223 where y represents the variation amplitude of the groundwater level [m]; x represents
224 the distance from the monitoring point to the riverbank [m]; a represents the change
225 of the Yangtze River water level within a specific period [m]; b represents the
226 attenuation coefficient [1/m]. For each monitoring profile shown in Fig. A1, eleven
227 polylines derived from the monthly water level differences are generated. Then those
228 polylines exhibiting abnormal patterns due to measurement errors or localized
229 hydrological influences are excluded. For each remaining polyline, Eq. (1) is applied
230 for fitting to inversely estimate the corresponding a and b values. The multiple b
231 values from each cross-section are then averaged to obtain \bar{b} , which is a new section-
232 specific attenuation coefficient for Eq. (1).

233 (3) Delineation of lateral influence extent. In hydrogeological practice, the
234 intensity of river influence on lateral groundwater dynamics is commonly
235 characterized by a dimensionless parameter R . Here, R is defined as the ratio of the

236 groundwater level fluctuation amplitude to the simultaneous river stage fluctuation
237 amplitude. It signifies the strength of the groundwater response to river fluctuations.

238 Therefore, by reformulating Equ. (1) and substituting the value of \bar{b} obtained
239 from Step (2), the formula for calculating the R value for each monitoring cross-
240 section can be expressed as

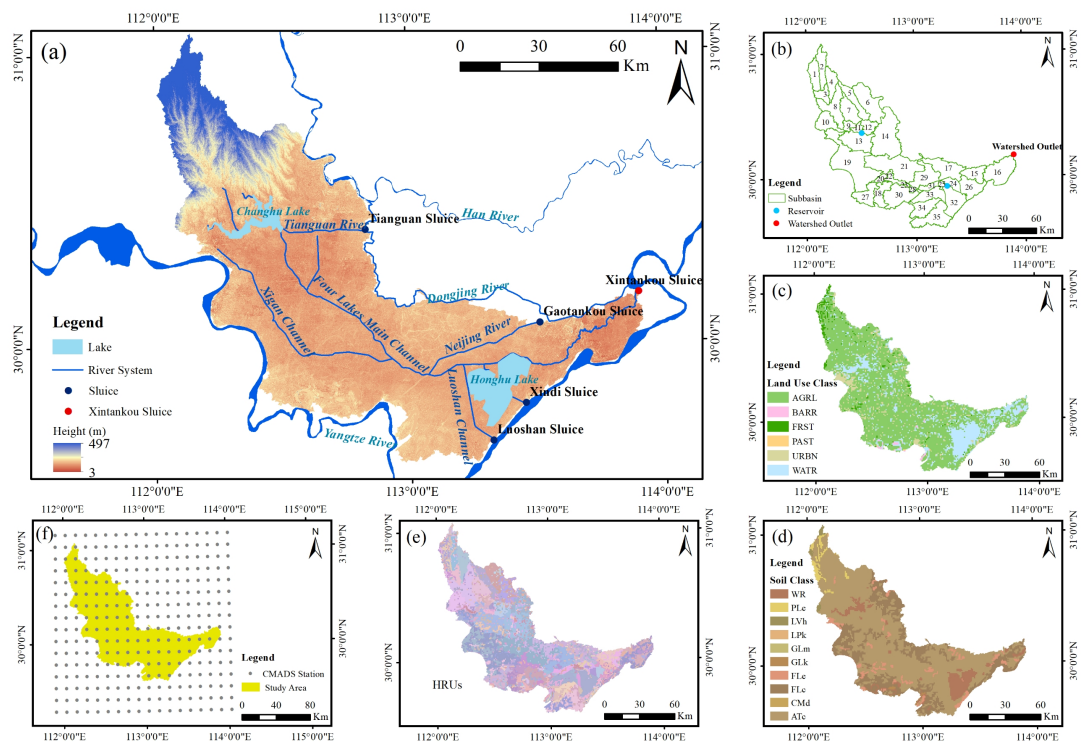
$$241 \quad R=y/a=e^{\bar{b}x} \quad (2)$$

242 According to established criteria (He and Cai, 1999), when $R < 0.02$, i.e., when
243 the groundwater fluctuation falls below 2% of the corresponding river stage
244 fluctuation, the river is considered to have no significant influence on the groundwater.
245 Thus, the distance from the riverbank corresponding to $R= 0.02$ was taken as the
246 maximum lateral influence extent of the Yangtze River on the confined aquifer.
247 Therefore, with the value of \bar{b} obtained in Step (2), the value of x , which indicates the
248 lateral influence range of the Yangtze River on groundwater, can be determined
249 inversely by assigning a value to R .

250 3.2.2 SWAT-MODFLOW coupling model for the Four-Lake Basin

251 After delineating the spatial response range through the data-driven approach,
252 one can clearly identify which surface water bodies, besides the Yangtze River,
253 significantly affect groundwater along the river, justifying the necessity of
254 considering them in a SW-GW interaction framework. The SWAT model for the
255 Four-Lake Basin was developed in ArcSWAT, with all data sources detailed in Table
256 1. The modeling framework began with watershed delineation, dividing the basin into
257 35 subbasins based on Digital Elevation Model (DEM) data and the river network.
258 Hydrologic Response Units (HRUs) were generated by overlaying land use
259 classification, soil types, and slope categories, ultimately producing 428 HRUs as

260 illustrated in Fig. 2. Meteorological data was extracted from the CAMADS v1.2
 261 dataset at 288 monitoring stations within and around the basin (Fig. 2f). The
 262 simulation spanned a three-year warm-up period (2008-2010), followed by calibration
 263 (2011-2014) and validation (2015-2016) phases, all performed at a monthly temporal
 264 resolution.

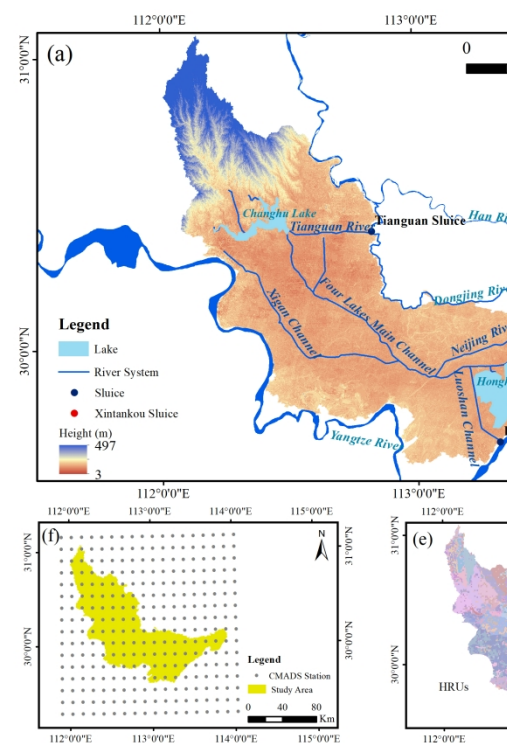


265

266 Figure 2: (a) Four-Lake Basin elevations, major water systems, and major sluices. (b) SWAT Model
 267 subbasins and watershed outlets. (c) Land use classification. (d) Soil classification. (e) SWAT Model
 268 HRUs. (f) CAMADS V1.2 stations.

269 A groundwater numerical simulation using the finite difference method was
 270 performed with Visual MODFLOW Flex 9.0. Based on regional hydrogeological
 271 conditions and borehole lithological data, a heterogeneous, anisotropic, and transient
 272 groundwater flow model for the Four-Lake Basin was generalized into three layers:

删除[k k]:



273 an unconfined aquifer, an aquitard, and a confined aquifer. The model was discretized
274 horizontally into 1 km × 1 km grids and vertically into three layers based on
275 hydrogeological stratification, resulting in 33,450 active cells. Hydrogeological
276 parameter zones, values, and boundary conditions are detailed in Fig. A2 and Table
277 A1 in the Appendix A.

278 The SWAT-MODFLOW coupled model was developed by establishing a one-
279 way correspondence between SWAT Hydrologic Response Units (HRUs) and
280 MODFLOW grid cells, in which SWAT provides spatially distributed groundwater
281 recharge to MODFLOW, while groundwater feedback to SWAT is not explicitly
282 simulated. This is reasonable because this study aims to investigate the interaction
283 rate between Yangtze River and groundwater instead of delineating the hydrodynamics
284 of surface water; additionally, under the intensive regulation of artificial drainage and
285 irrigation pumping stations in the Four-Lake Basin, the effect of surface water
286 recharge on groundwater is substantially greater than the influence of groundwater
287 discharge on surface water. The calibrated SWAT model provided monthly
288 groundwater recharge (GW_RCHG) and actual evapotranspiration data, which were
289 then assigned to the corresponding MODFLOW cells. These outputs were directly
290 used as inputs for the Recharge (RCH) and Evapotranspiration (EVT) packages in
291 MODFLOW, thereby driving the groundwater flow simulation.

292 **4 Results and Discussion**

293 **4.1 The influence range of the Yangtze River on lateral groundwater**

294 The response of confined groundwater levels to fluctuations in the Yangtze River
295 stage was evaluated across seven monitoring profiles (ZJ, JZ, JL, JLX1, JLX2, HH1,
296 and HH2) at increasing distances (x) from the river. As illustrated in Fig. A1, the

297 sensitivity of groundwater levels to river stage diminishes with distance. One notable
 298 deviation is observed along the ZJ profile, where anomalously large groundwater
 299 fluctuations occur 5~10 km from the riverbank, possibly due to local hydrogeological
 300 heterogeneity or anthropogenic influences. The amplitude-distance relationships for
 301 both the Yangtze River and groundwater levels, fitted using Equation (1) across all
 302 seven monitoring profiles, are shown in Fig. A3 in the Appendix A. For clarity,
 303 results from a representative period of the year are displayed. All fitted curves
 304 demonstrate a high goodness-of-fit ($R^2 > 0.9$), indicating highly reliable correlations.
 305 Based on these relationships, the range of estimated b values and the corresponding
 306 fitting equations for each profile were calculated, as summarized in Table 2.

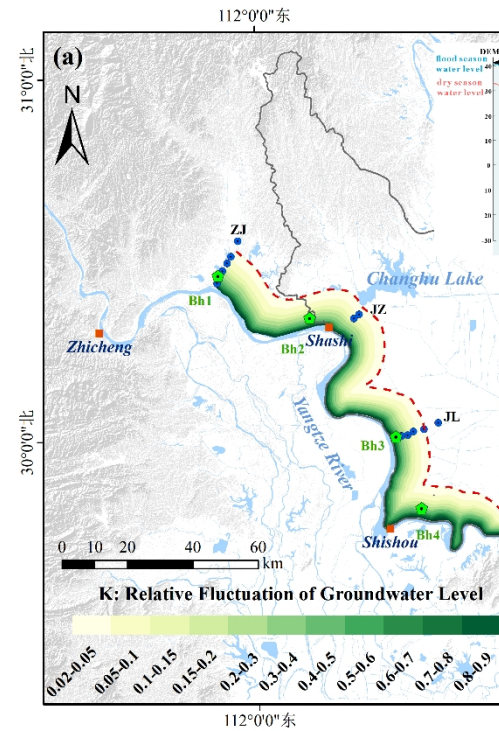
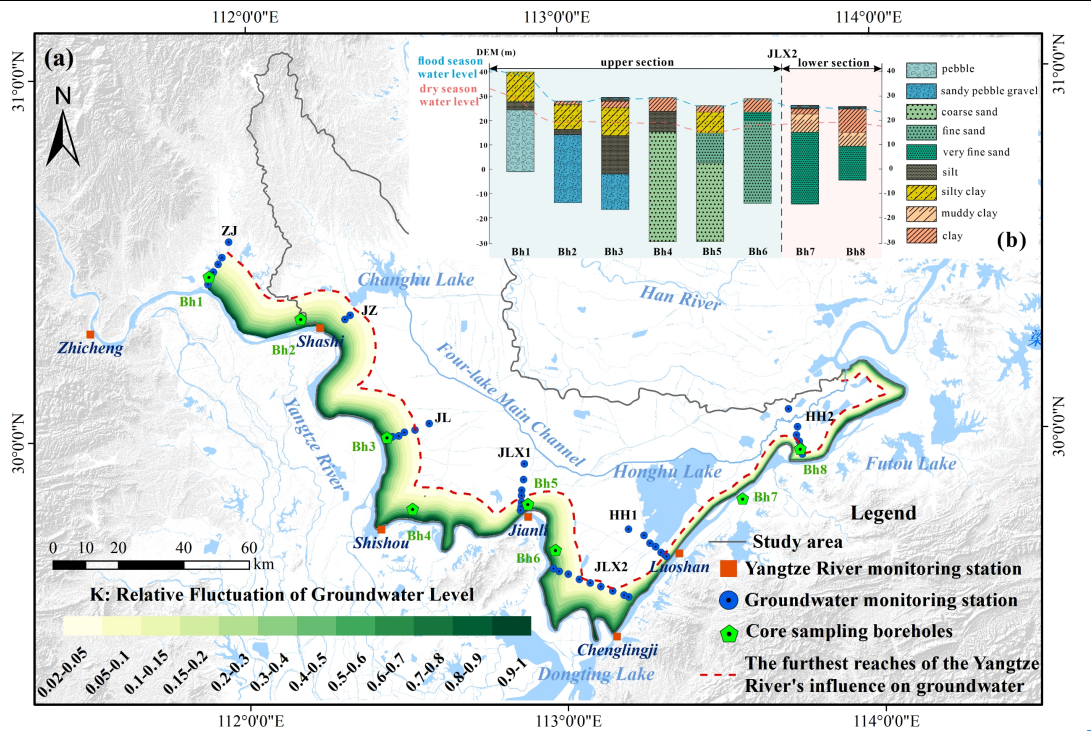
307 Table 2 The range of estimated values of b and corresponding fitting equations for each profile

Section	The range of estimated values of b	Attenuation fitting equation
ZJ	-0.1271~-0.4081	$R_{zj}=e^{-0.3064x}$
JZ	-0.3375~-0.3569	$R_{zj}=e^{-0.3463x}$
JL	-0.3272~-0.4432	$R_{jl}=e^{-0.3687x}$
JLX1	-0.556~-0.8021	$R_{jlx1}=e^{-0.6935x}$
JLX2	-0.2546~-0.5289	$R_{jlx2}=e^{-0.3824x}$
HH1	-1.7839~-2.5305	$R_{hh1}=e^{-2.0203x}$
HH2	-1.4486~-2.0477	$R_{hh2}=e^{-1.7638x}$

308 To quantify the intensity and maximum lateral extent of the Yangtze River's
 309 influence on the adjacent confined aquifer, the criterion defined in step (3) was
 310 applied. According to this criterion, the distance x corresponding to a relative
 311 groundwater fluctuation (R) of 0.02 represents the maximum influence distance.
 312 Table 3 presents the calculated maximum influence distances and the mean
 313 attenuation coefficients (\bar{b}) for each monitoring profile. At the same time, Fig. 3
 314 visually depicts the influence distances across a range of R values, including this
 315 maximum extent.

316 Table 3 Distance x from the riverbank corresponding to $R = 0.02$ and average attenuation coefficient \bar{b}
 317 for each profile.

Profiles	ZJ	JZ	JL	JLX1	JLX2	HH1	HH2
x	12.77	11.30	10.61	5.64	10.23	1.94	2.22
\bar{b}	-0.3064	-0.3463	-0.3687	-0.6935	-0.3824	-2.0203	-1.7638



318
 319 Figure 3: (a) Different degrees and ranges of influence of the Yangtze River on the lateral confined
 320 groundwater in the Four-Lake Basin. (b) Lithologic logs of boreholes along the Yangtze River in the
 321 Four-Lake Basin.

322 As summarized in Table 3 and Fig. 3, the influences of the Yangtze River on the
 323 confined groundwater in the Four-Lake Basin exhibits distinct spatial zoning, with
 324 JLX2 acting as a critical boundary. Consequently, the study area is divided into two
 325 independent segments, i.e., the ZJ-JLX2 reach and the JLX2-HH2 reach, which can
 326 be characterized by three key features:

删除[k k]:

327 (1) Extended influence range: The ZJ-JLX2 segment shows a smaller attenuation
328 coefficient (b) and a maximum influence distance of 12.77 km (Table 3), indicating
329 more efficient pressure transmission through the aquifer system than in the JLX2-
330 HH2 reach downstream.

331 (2) Hydraulic head differences primarily drive groundwater response: Due to its
332 proximity to the TGD, the ZJ-JLX2 segment experiences amplified river-stage
333 fluctuations that propagate over long distances. In contrast, the JLX2-HH2 segment
334 lies downstream of the Yangtze River after regulation by Dongting Lake, where river
335 stage variations are markedly dampened, leading to a shorter propagation distance of
336 hydraulic signals. Note that the Yangtze River's lateral influence range at the JLX1
337 cross-section is only 5.64 km, which differs significantly from other cross-sections
338 within the reach. This is because the JLX1 cross-section is located precisely at the
339 point where the Yangtze River channel bends inward toward the interior of the Four-
340 Lake Basin. The proximity to both the internal water system of the basin and the
341 densely populated area of Jianli City results in a significantly weak response of the
342 JLX1 cross-section to water level fluctuations in the Yangtze River.

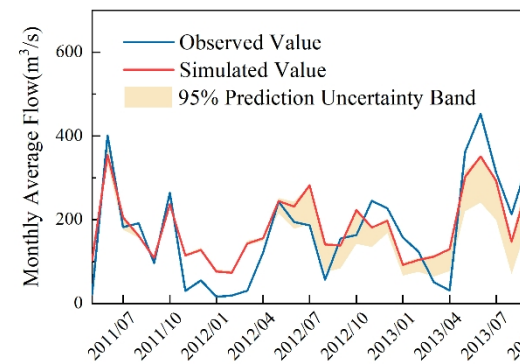
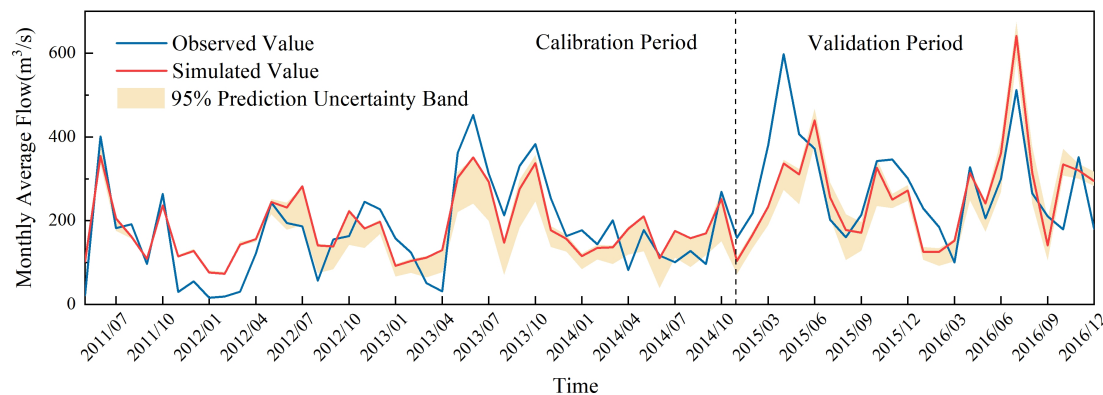
343 (3) Favorable hydrogeological conditions: The JL profile, representative of the
344 ZJ-JLX2 segment, consists of highly permeable gravel-cobble formations (Fig. 1e),
345 which minimize hydraulic head loss and support long-distance transmission of river-
346 induced fluctuations. Although the 2021 Yangtze River Sediment Bulletin indicates
347 that the river incises into the confined aquifer in the JLX2-HH2 segment, Fig. 1f
348 shows that near the profiles HH1 and HH2, the aquifer materials are dominated by
349 fine sands. The resulting lower permeability and higher flow resistance cause rapid
350 attenuation of head fluctuations, thus restricting the lateral extent of the river's
351 influence.

352 Furthermore, the proximity of Honghu Lake to the HH1 and HH2 segment
353 warrants consideration. Although not in direct hydraulic contact with the confined
354 aquifer, this extensive shallow lake interacts dynamically with the overlying phreatic
355 aquifer. As shown in Fig. 1f, the shallow aquitard in the vicinity of Honghu Lake
356 exhibits significant spatiotemporal heterogeneity in thickness, facilitating localized
357 hydraulic connectivity between the unconfined and confined aquifer systems. Under
358 these conditions, Honghu Lake acts as a hydrological buffer; that is, its relatively
359 stable water levels attenuate the transmission of Yangtze River stage fluctuations to
360 adjacent groundwater systems. In addition, we generated the results shown in Fig. 3
361 for the period from 2022 to 2024, and compared the lateral influence range of the
362 Yangtze River on coastal groundwater for each year from 2021 to 2024 (as shown in
363 Fig. A4). The results indicate that this lateral influence range has not changed
364 significantly in recent years, which may be attributed to the fact that annual
365 precipitation in this region has remained consistently between 1000 and 1200
366 millimeters.

367 Based on the analysis of data-driven, the high goodness-of-fit ($R^2 > 0.9$) across
368 all profiles suggests a stable groundwater response to Yangtze River stage
369 fluctuations. Moreover, the derived spatial variation in attenuation coefficients and
370 influence distances is consistent with observed along-river differences in
371 hydrogeological conditions, providing confidence in the robustness of this approach.
372 These results also serve as an independent reference for interpreting the spatial
373 patterns simulated by the coupled SWAT-MODFLOW model in later sections. It is
374 also worth noting that since the establishment of the riparian monitoring network,
375 annual precipitation in the study area has shown limited variability. As a result,
376 findings from years other than 2021 do not differ substantially from those of 2021,
377 which justifies its selection as a representative year in this study.

378 **4.2 Validation of the SWAT-MODFLOW model**

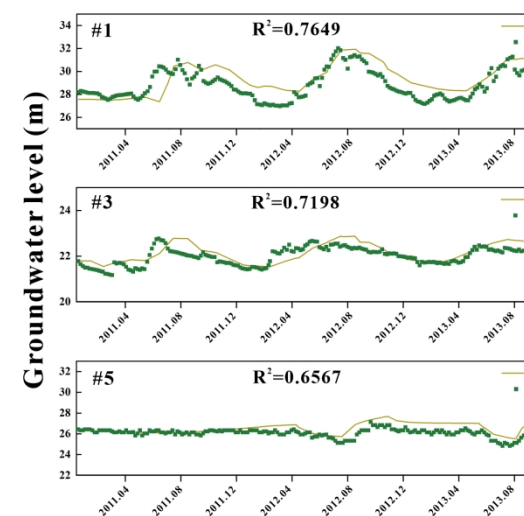
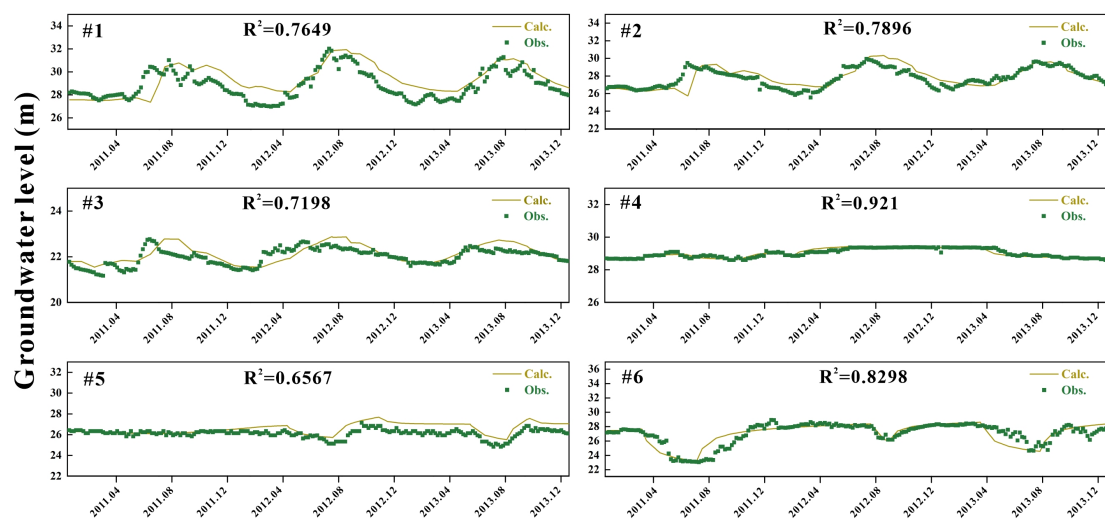
379 Clearly, the results in Section 4.1 demonstrate that the lateral influence range of
380 the Yangtze River encompasses various surface water bodies, highlighting the
381 necessity of using the SWAT-MODFLOW model. The SWAT model for the Four-
382 Lake Basin was calibrated and evaluated using SWAT-CUP, a dedicated tool for
383 parameter calibration and uncertainty analysis for SWAT model. Sensitivity analysis,
384 a key step within this process, was conducted with the SUFI-2 algorithm to identify
385 the parameters exerting the greatest influence on the model outputs (Khaleghi et al.,
386 2024). A total of 17 key parameters were selected for sensitivity analysis and
387 calibration, with 1,000 iterations conducted to optimize model performance. Table A2
388 summarizes the calibrated parameters, their fitted values, and sensitivity ranks.
389 Monthly surface runoff data from the Xintankou station (outlet of sub-basin 16) from
390 2011 to 2016 were used for both model calibration (2011-2014) and validation (2015-
391 2016). As shown in Fig. 4, the model performed well, achieving Nash-Sutcliffe
392 efficiency (NSE) values of 0.7 and 0.65 during calibration and validation, respectively,
393 and R^2 values of 0.76 (calibration) and 0.67 (validation), indicating satisfactory
394 agreement between simulated and observed runoff.



395
396 Figure 4: The fitting between the simulated monthly flow that has been calibrated and the observed one.

删除[k k]:

397 The coupled SWAT-MODFLOW model was calibrated against observed
 398 groundwater levels from six monitoring wells from 2011 to 2013 distributed near
 399 Yangtze River (Fig. 1). As shown in Fig. 5, the simulated groundwater levels agree
 400 well with the observed values throughout the simulation period, demonstrating the
 401 capability of the model to reproduce regional groundwater dynamics. These results
 402 confirm that the integrated model reliably captures the key characteristics of surface
 403 water-groundwater interactions in the Four-Lake Basin.



404

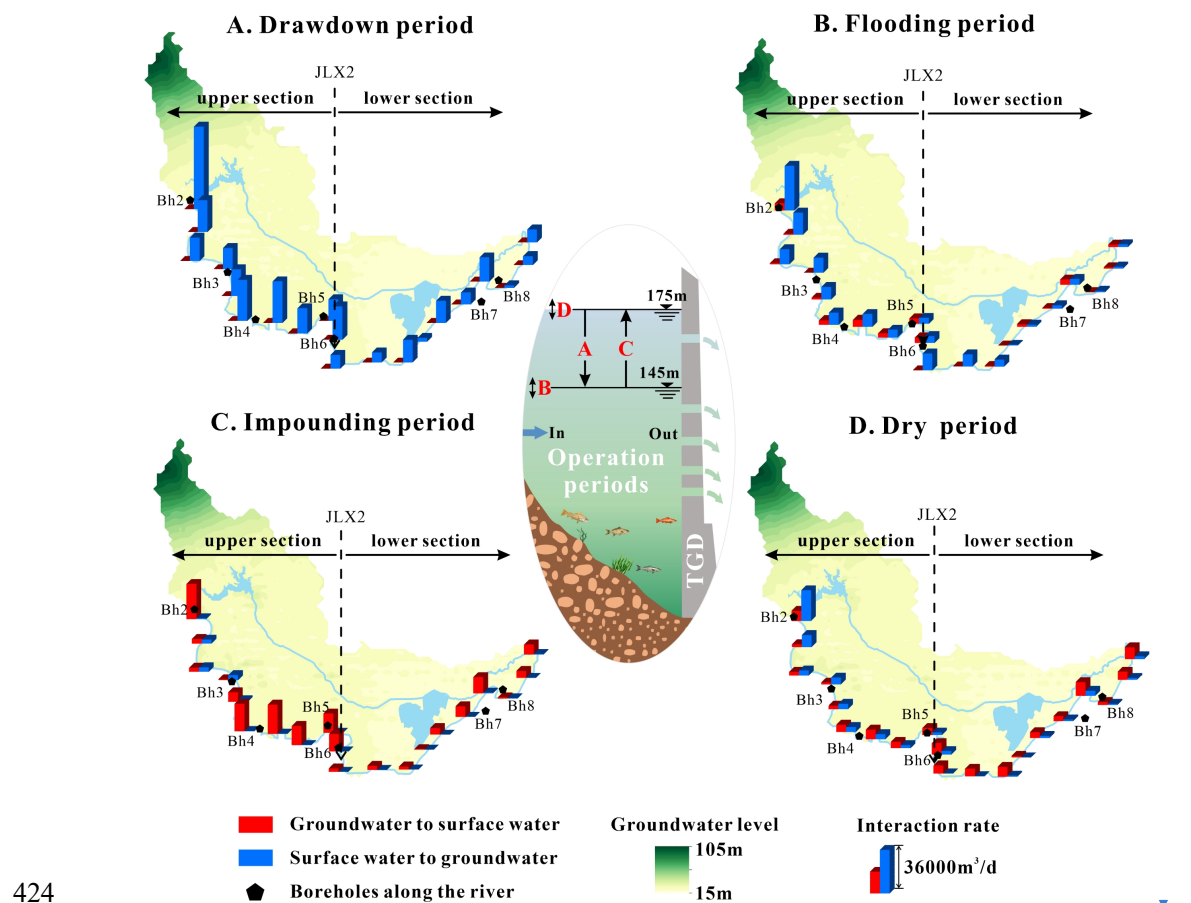
405 Figure 5: Fitting between the Observed groundwater levels and the calculated ones at the monitoring
 406 wells during the simulated period.

407 4.3 Yangtze River-groundwater interaction under TGD regulation: 408 Spatiotemporal patterns

409 Figure 6 illustrates the daily exchange volume between the Yangtze River and
 410 groundwater in the mainstream within the Four-Lake Basin, calculated by the SWAT-
 411 MODFLOW model at 15-km intervals. The relative magnitudes are represented by
 412 bar charts, with blue and red indicating groundwater recharge from and discharge to
 413 the Yangtze River, respectively. The four subplots correspond to the four scheduling

删除[k k]:

414 periods of the TGD: (1) Drawdown period. This period refers to the pre-flood water
415 release phase, during which the water level of the TGD is lowered below the flood
416 limit level through controlled discharge to prepare for flood peak retention and
417 attenuation; (2) Flooding period. This period represents the subsequent flood season,
418 during which the reservoir intercepts floods and adjusts the timing of downstream
419 flood peaks; (3) Impounding period. This period denotes the post-flood water storage
420 phase, where water at the end of the flood season is stored for use during dry periods;
421 (4) Dry period. This period is set for the water stored in the previous period to release
422 to supplement downstream flow during dry seasons. The results in the figure represent
423 the daily average exchange rate over all days within each operational period.

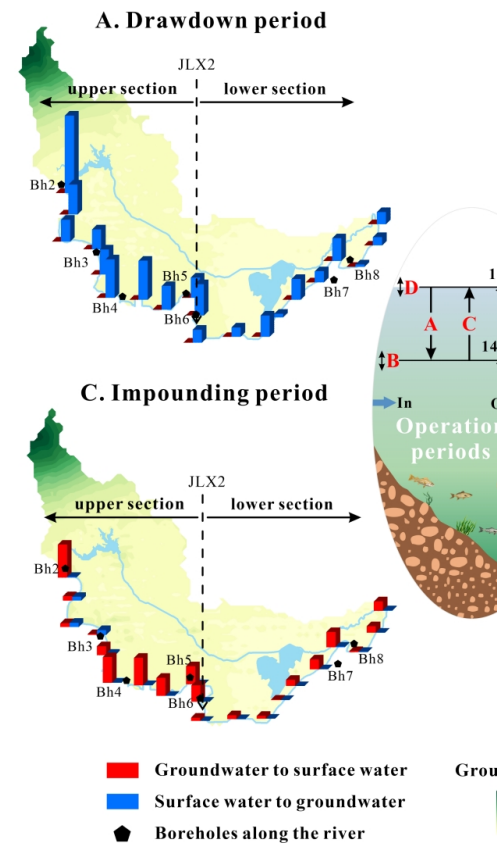


424

425 Figure 6: Spatial variations in interaction rates (average of 2011 and 2013, m^3/d) between the Yangtze
 426 River and groundwater in the Four-Lake Basin during the four operational periods of the TGD. Red
 427 histograms denote groundwater discharge to surface water; blue histograms denote surface-water
 428 recharge to groundwater. TGD operational periods: A-Drawdown period, B-Flooding period, C-
 429 Impounding period and D-Dry period. The vertical dashed line indicates a spatial demarcation for
 430 different interaction patterns along the river reach.

431 As shown in Fig. 6, river-to-aquifer recharge dominates during both the
 432 drawdown period and the flooding period, while aquifer-to-river discharge prevails in
 433 the other two periods. Moreover, the recharge rate during the drawdown period is
 434 significantly higher than that during the flooding period. It occurs because during the
 435 drawdown period, the TGD gradually lowers the reservoir level from 175 m at the end

删除[k k]:



436 of the previous winter to below 145 m (referenced to the Yellow Sea Datum) and
437 releases the incoming spring flows upstream. The substantial outflow leads to a
438 marked rise in the downstream river stage, amplifying the hydraulic gradient between
439 the river and adjacent groundwater and driving strong river-to-aquifer recharge.
440 During the flooding period, groundwater levels are considerably elevated due to
441 rainfall infiltration and surface water recharge in the Four-Lake basin, which have
442 been confirmed by our SWAT-MODFLOW simulation. Additionally, TGD
443 operations during this period aim to attenuate downstream flood peaks for safety,
444 thereby significantly reducing the hydraulic gradient between the river and
445 groundwater compared to that during the drawdown period. It explains why the
446 apparent river-groundwater exchange is weaker during the hydrologically more
447 dynamic flooding period, as observed in Fig. 6b.

448 The intensity of aquifer-to-river discharge is higher during the impounding
449 period than during the dry period. This difference arises because during the
450 impounding period, groundwater levels remain elevated following the end of the
451 flood season, while the TGD begins to impound upstream water in preparation for the
452 dry-season water supply. This process enlarges the hydraulic gradient between
453 groundwater and the Yangtze River. In contrast, during the dry period, groundwater
454 levels have declined, and the TGD releases water to supplement downstream flow,
455 which reduces the hydraulic gradient between groundwater and the river. It explains
456 why the aquifer-to-river discharge intensity is stronger during the impounding period
457 than during the dry period.

458 In addition, dividing the Yangtze River at the JLX2 monitoring section into an
459 "upper section" and a "lower section" (as shown in Fig. 6) reveals consistently higher
460 exchange rates in the upper one. This pattern arises because the upper section is closer
461 to and more influenced by TGD regulation than the lower section, leading to larger

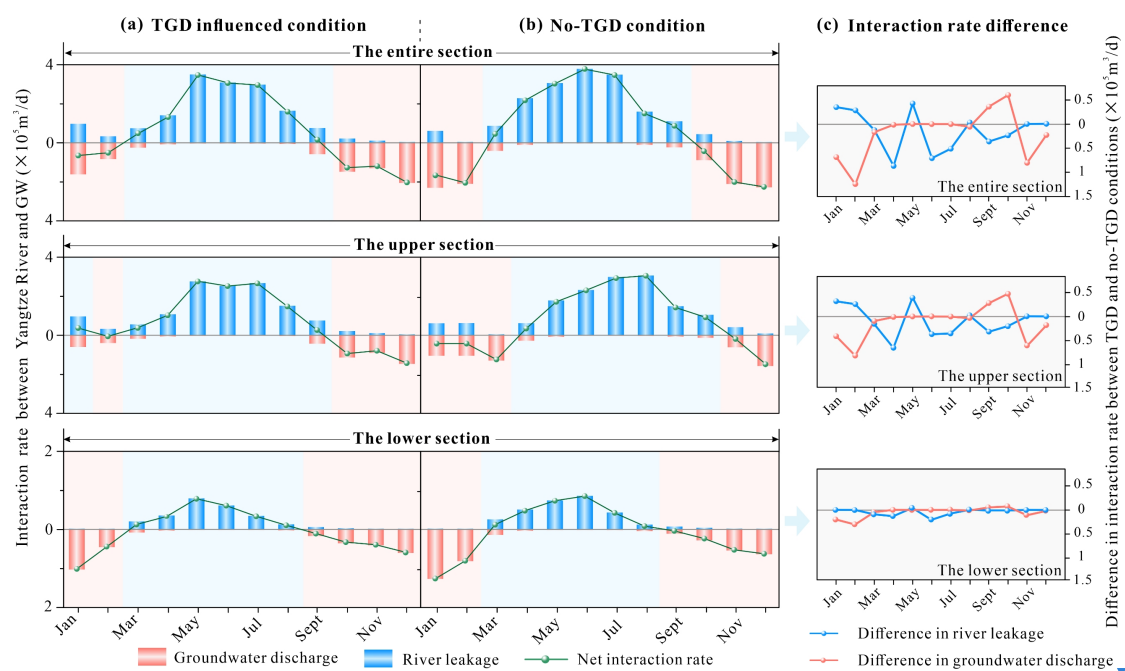
462 stage fluctuations and weaker along-stream attenuation, which together enhance the
463 hydraulic gradient. In contrast, the lower section, characterized by a wider channel
464 and greater hydraulic connectivity with tributaries, exhibit a comparatively weaker
465 response to the Three Gorges Dam operations. As shown in Fig. A5 in the Appendix
466 A, wavelet coherence analysis reveals that with increasing distance from the TGD, the
467 downstream river stage exhibits a progressive damping in its response to reservoir
468 release variations, accompanied by a lengthening phase lag (see Appendix A).
469 Moreover, the along-river lithology profile in Fig. 3b reveals a distinct shift in aquifer
470 composition: the upstream banks are dominated by highly permeable gravel and
471 coarse sand, which sharply contrasts with the less permeable fine sand that constitutes
472 the downstream deposits. The strong heterogeneity of the riparian stratigraphy is also
473 a significant factor contributing to the weaker downstream interactive strength
474 compared to that upstream. Notably, the spatial contrast in exchange intensity
475 revealed by the SWAT-MODFLOW simulations is consistent with the lateral
476 influence patterns identified in Section 4.1, indicating that along-river geological
477 heterogeneity and Yangtze River stage variability jointly control the interaction
478 between lateral groundwater and the Yangtze River.

删除[Zhu Qi]: 4

479 **4.4 Yangtze River-groundwater interaction with and without TGD: A** 480 **counterfactual comparison**

481 Against the backdrop of numerous factors influencing Yangtze River-
482 groundwater interactions, this study isolated the effect of TGD regulation by
483 implementing simulated "no-TGD" river stages from Wang et al. (2013) in the
484 SWAT-MODFLOW model. All other input data, such as precipitation, evaporation,
485 groundwater levels, and tributary/lake stages, remained unchanged. This setup
486 produced the results of river leakage to groundwater and groundwater discharge to

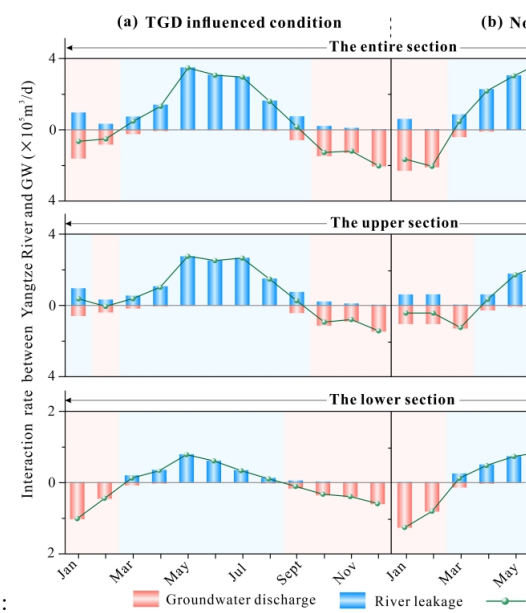
487 river shown in Figures 7(a) and 7(b), respectively: they illustrate the monthly
 488 variations in daily exchange rates between the Yangtze River and groundwater for the
 489 upper section, lower section, and the entire mainstream of the Four-Lake basin,
 490 demarcated by the JLX2 monitoring section. Here, the daily interaction rate represents
 491 the monthly total interaction amount averaged over all the days in that month,
 492 visualized using bar charts: red bars indicate aquifer-to-river discharge, and blue bars
 493 represent river-to-aquifer recharge. The green line graph in Figs. 7(a) and 7(b) depict
 494 the net daily exchange, calculated as river leakage minus groundwater discharge. Fig.
 495 7(a) shows simulation results influenced by TGD operation (corresponding to those in
 496 Fig. 6), while Fig. 7(b) presents those without TGD. By subtracting the daily
 497 interaction rates in Fig. 7(b) from those in Fig. 7(a), we obtain the differences in these
 498 rates between the scenarios with and without the TGD, as shown in Fig. 7(c).



499

500 Figure 7: Temporal variations in the river leakage rates, groundwater discharge rates and net exchange
 501 rates under TGD-influenced (a) and no-TGD conditions (b) between the Yangtze River and
 502 groundwater. Fluxes are positive for river leakage to the aquifer and negative for groundwater

删除[k k]:



503 discharge to the river. (c) Interaction rate difference between TGD and no-TGD conditions in river
504 leakage and groundwater discharge. More detailed information can be found in Table A3.

505 Figure 7(b) shows that regardless of TGD operation, the Yangtze Rive leakage to
506 groundwater dominates from March to September in both the upper and lower
507 sections of the Four-Lake basin. In contrast, groundwater discharge to the Yangzte
508 River prevails from October to February of the following year. Across the entire
509 section of stream, the peak net exchange rate occurs in June, reaching $3.77 \times 10^5 \text{ m}^3/\text{d}$.
510 Spatially, the net flow direction (river leakage versus groundwater discharge) differs
511 between the upper and lower sections. In the upper section, the rate of river leakage to
512 groundwater consistently exceeds the discharge rate, regardless of TGD regulation.

513 With a comparison between Figs. 7(a) and 7(b) by calculating the average net
514 exchange rates for both flooding season (from June to September) and dry period
515 (from November to April), one can find that TGD operations significantly suppress
516 the natural river-groundwater exchange. Under TGD regulation, the net exchange rate
517 across the entire section decreased by 19.3% and 41.8% during the flooding and dry
518 periods, respectively, compared to natural conditions. This suppression was more
519 pronounced in the upper section, where the net exchange dropped by 40.6% during
520 the dry period, contrasting with a decrease of 23.8% in the lower section. In addition,
521 it can be visually inferred from Fig. 7(c) that a considerable number of values lie
522 below zero. This indicates that, compared to the natural conditions, TGD operations
523 lead to a reduction in river leakage to groundwater for nine months of the year and a
524 decrease in groundwater discharge to the river for ten months in the upper section.
525 Notably, in the lower section, the fluxes in both directions (river leakage and
526 groundwater discharge) are reduced throughout nearly the entire year.

527 These findings demonstrate that the TGD attenuates flood peaks and elevates
528 low flows, thereby reducing the seasonal amplitude of river stages and narrowing the

529 river-aquifer hydraulic gradient. Consequently, the exchange dynamics become more
530 balanced and stable. The upper section, being directly subject to regulatory releases,
531 exhibits a more pronounced response in net exchange, particularly during the dry
532 season. As also evident from the mapped zone of the Yangtze River's lateral influence
533 on groundwater in Fig. 3, the groundwater response to river stage changes is visibly
534 weaker in the lower section, particularly near Honghu Lake, compared to the upper
535 section. As shown by the net interaction curve for the upper section (Fig. 7), the
536 period from January to March, which was naturally characterized by groundwater
537 discharge to the river, transitions to a state of weak river leakage to the aquifer
538 following the TGD-induced rise in dry-season river stage. This flow reversal occurs
539 because the dry-season hydraulic gradient is inherently small; thus, even a modest
540 stage increase can induce a substantial relative change, making the regulatory
541 influence more pronounced during dry months than in the flood season.

542 **5 Limitations and Future Work**

543 This study has its potential sources of uncertainty, which arises from the spatial
544 sparsity of observation well data used for model calibration and the inability of the
545 one-way coupled model to simulate groundwater discharge to surface water. Besides,
546 several limitations should be acknowledged; **Firstly**, the lateral influence distance of
547 the Yangtze River was analyzed using the full-year observed amplitude of both river
548 stage and groundwater level fluctuations, making it difficult to interpret how this
549 result varies across different seasons or hydrological year types. Therefore, a more
550 detailed characterization of intra-annual variability would require longer monitoring
551 records with higher temporal resolution, which will be addressed in future work.
552 **Secondly**, in such a riparian wetland environment, the sources of groundwater

删除[Zhu Qi]: . Besides, two limitations should be acknowledged

删除[Zhu Qi]: on one hand

删除[Zhu Qi]: On the other hand

553 recharge along the riverbank has not been analyzed in detail. Future studies will
554 therefore consider tracer-based investigations to further evaluate groundwater sources
555 associated with major lakes, rivers, wetlands, and localized upland areas in the Four-
556 Lake Basin. Thirdly, Regarding the spatial influence of the Yangtze River on lateral
557 groundwater, providing a calculation result without the TGD, similar to the numerical
558 modeling approach, would greatly help deepen the discussion on this topic. However,
559 the scarcity of observed groundwater data prior to the construction of the TGD has
560 constrained the successful implementation of this idea.

561 **6 Conclusion**

562 This study integrated large-scale monitoring data from multiple profiles along
563 the Yangtze River in the Four-Lake Basin, on which a spatial response analysis of
564 water levels was performed followed by a coupled surface water-groundwater
565 modeling framework. Then, the interactions between the Yangtze River and
566 groundwater were systematically investigated through both qualitative and
567 quantitative analyses. The key findings are as follows:

568 (1) Spatial variability of the Yangtze River influence. The lateral influence zone
569 of the Yangtze River on groundwater in the Four-Lake Basin has been quantified for
570 the first time, revealing a band-like pattern with a high degree of spatial heterogeneity.
571 The lateral influence range varies from 1.94 km (HH1 profile) to 12.77 km (ZJ profile)
572 across the Four-Lake Basin.

573 (2) Performance of the newly proposed model. Given the significant influence of
574 rainfall and the surface water network on groundwater in the Four-Lake basin, the
575 SWAT-MODFLOW model is capable of accurately quantifying the exchange fluxes
576 between the Yangtze River and groundwater.

577 (3) Spatial-temporal interaction dynamics between the Yangzte River and
578 groundwater. Temporally, the Yangtze River leakage to groundwater is greater during
579 the drawdown period than during the flooding period. Conversely, groundwater
580 discharge to the Yangzte river is higher in the impounding period than in the dry
581 period. This dynamic is dictated by the combined effects of seasonal TGD regulation
582 and the local hydroclimate. Spatially, the interaction intensity between the Yangtze
583 River and groundwater is markedly higher in the upper section of the Four-Lake
584 Basin than the lower section, which is attributed to the integrated influences of the
585 TGD, the thalweg configuration, and riparian hydrogeology.

586 (4) The impacts of the TGD operation on the Yangtze River-groundwater
587 interaction. By modulating river stages, TGD operations reduce temporal variability
588 in Yangtze River-groundwater exchange rates, thereby promoting more balanced and
589 stable dynamics. This effect is most direct and pronounced in the upper section during
590 the dry period, whereas its influence attenuates downstream.

591

592

593 **Appendix A**

594

595

Table A1 Aquifer hydrogeologic parameters for MODFLOW model.

Parameter Zone	Horizontal Conductivity		Vertical Conductivity		Specific Yield	Specific Storage
	K_x and K_y (m/d)		K_z (m/d)		S_y	S_s (L ⁻¹)
	Unconfined Aquifer	Confined Aquifer	Unconfined Aquifer	Confined Aquifer	Unconfined Aquifer	Confined Aquifer
1	1.00	9.75	0.150	1.1		0.0004
2	1.5	16	0.302	1.6	0.021	0.0022
3	0.79	7.7	0.120	0.85		0.001
4	0.54	4.9	0.081	0.57		0.0023

596

597

598

Table A2 SWAT model calibrated parameters with adjusted values and sensitivity ranking.

Symbol	scale	Calibrated Value	<i>t</i> -value	<i>p</i> -value	Sensibility
GWQMN	0-5000	186.90	-30.89	0.00	1
REVAPMN	0-500	188.31	15.60	0.00	2
GW_DELAY	0-500	232.39	-1.97	0.05	3
CH_N2	-0.01-0.3	0.11	1.91	0.06	4
SOL_BD	0.9-2.5	1.13	1.79	0.07	5
CH_N1	0.01-30	20.30	-1.48	0.14	6
CH_K2	-0.01-500	27.39	-1.22	0.22	7
SURLAG	0.05-24	15.11	-1.21	0.23	8
GW_REVAP	0.02-0.2	0.17	-1.20	0.23	9
SOL_AWC	0-1	0.00	0.90	0.37	10
ESCO	0.01-1	0.36	0.88	0.38	11
OV_N	0.01-30	17.89	-0.81	0.42	12
ALPHA_BNK	0-1	0.33	-0.79	0.43	13
ALPHA_BF	0-1	0.22	-0.47	0.64	14
SOL_K	0-2000	1766.62	0.38	0.70	15
EPCO	0.01-1	0.38	0.16	0.87	16
CN2	35-98	35.34	-0.01	0.99	17

599

600 Table A3 Average river leakage, groundwater discharge, and net exchange rates (average of 2011 to
601 2013) under TGD regulated operation and natural conditions between the Yangtze River and
602 groundwater for the entire section, upper section, and lower section.

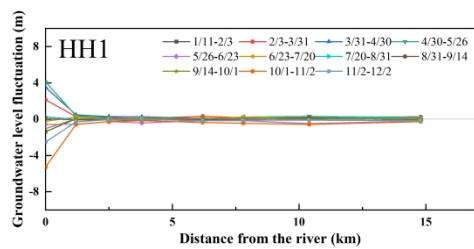
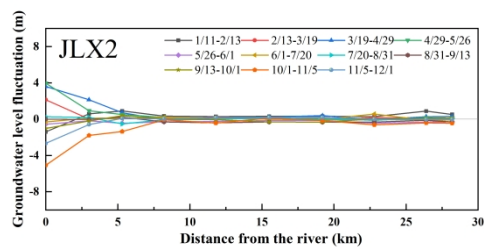
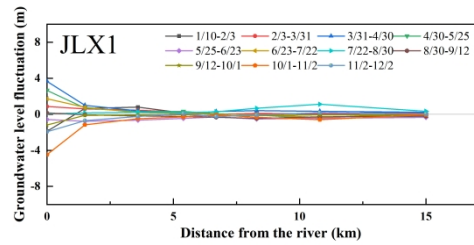
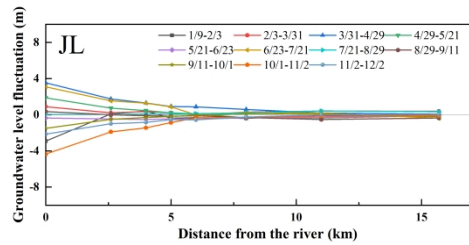
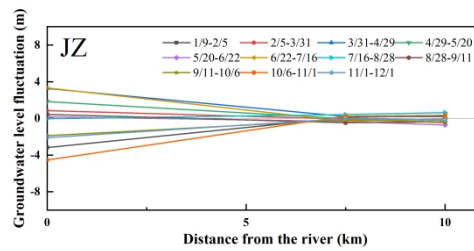
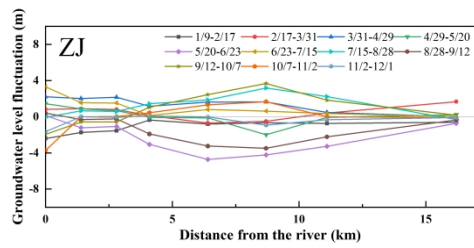
Month	TGD regulated operation (m ³ /d)			Natural condition (m ³ /d)		
	GW to SW interaction rate	SW to GW interaction rate	Net interaction rate	GW to SW interaction rate	SW to GW interaction rate	Net interaction rate
The entire section						
January	160398.61	95125.29	-65273.32	228615.16	60134.45	-168480.71
February	82495.96	31721.82	-50774.14	207866.07	3207.19	-204658.88
March	23711.71	72382.68	48670.97	39499.77	85539.23	46039.45
April	6623.12	138788.77	132165.65	8323.54	226616.07	218292.53
May	243.95	346652.48	346408.53	392.89	303461.94	303069.04
June	164.13	306211.00	306046.87	177.75	376947.00	376769.25
July	820.53	296601.61	295781.08	738.01	347322.58	346584.57
August	3511.69	161664.84	158153.15	8772.14	158542.26	149770.11
September	57918.17	73367.00	15448.83	21667.64	109546.30	87878.66
October	147234.71	19725.15	-127509.56	86604.52	43101.06	-43503.45
November	128486.87	8695.77	-119791.10	208785.13	8053.23	-200731.90
December	204551.52	1709.64	-202841.88	227181.03	1014.45	-226166.58
The upper section						
January	58348.03	95037.48	36689.45	102956.55	60063.03	-42893.52
February	38014.14	31633.79	-6380.36	127649.18	3134.64	-124514.54
March	16301.00	53726.03	37425.03	26561.48	60730.62	34169.13
April	4151.07	106185.73	102034.66	5809.77	176407.07	170597.30
May	119.41	273851.55	273732.14	193.20	229956.61	229763.42
June	0.00	251251.33	251251.33	43.90	291955.00	291911.10
July	189.88	265419.35	265229.48	195.26	304419.35	304224.09
August	1747.66	149041.61	147293.95	5534.11	146825.81	141291.70
September	41711.41	67952.03	26240.62	11612.61	103078.03	91465.43
October	112226.70	17772.32	-94454.38	59672.18	39762.87	-19909.31
November	88397.23	8008.71	-80388.52	155803.43	7426.35	-148377.08
December	144907.90	1609.14	-143298.76	164598.90	935.00	-163663.90
The lower section						
January	102049.81	88.41	-101961.40	125658.55	71.12	-125587.42
February	44481.75	88.01	-44393.74	80217.18	72.57	-80144.61

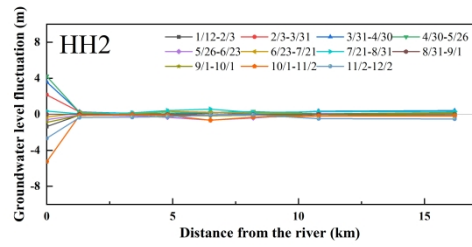
March	7410.79	19464.46	12053.67	12938.26	24809.01	11870.76
April	2472.04	34925.19	32453.15	2513.73	50209.80	47696.07
May	124.54	78462.61	78338.07	199.69	73506.32	73306.63
June	164.13	60520.87	60356.74	133.85	84992.97	84859.12
July	630.65	34033.13	33402.48	542.75	42902.87	42360.12
August	1764.04	12076.83	10312.79	3238.03	11716.11	8478.07
September	16207.16	4955.09	-11252.07	10055.03	6469.54	-3585.49
October	35008.08	1889.88	-33118.21	26932.46	3337.93	-23594.54
November	40089.60	684.73	-39404.87	52981.83	626.87	-52354.95
December	59643.16	100.48	-59542.68	62582.29	79.45	-62502.84

603

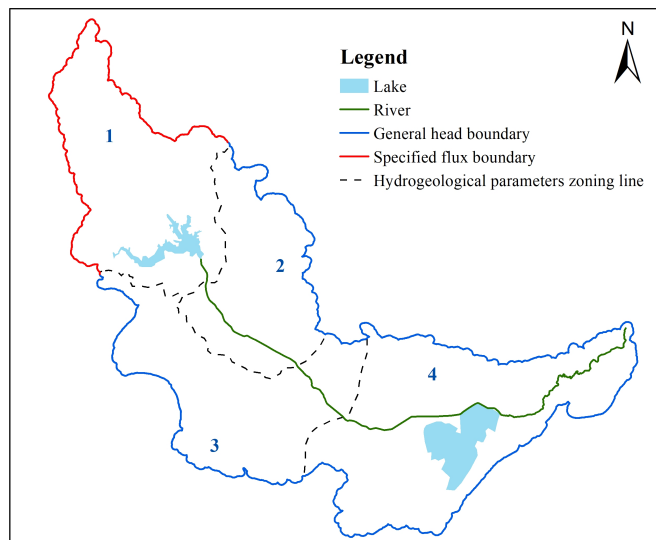
604

605

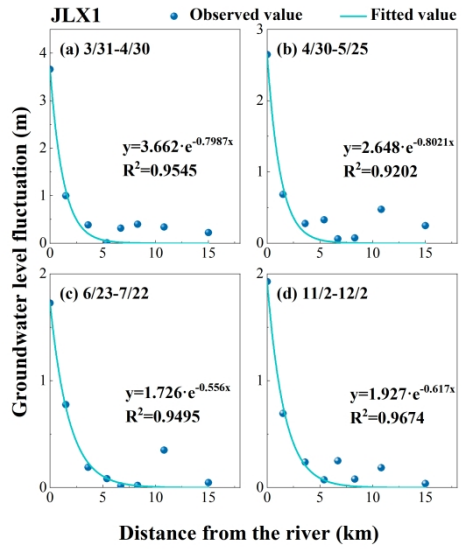
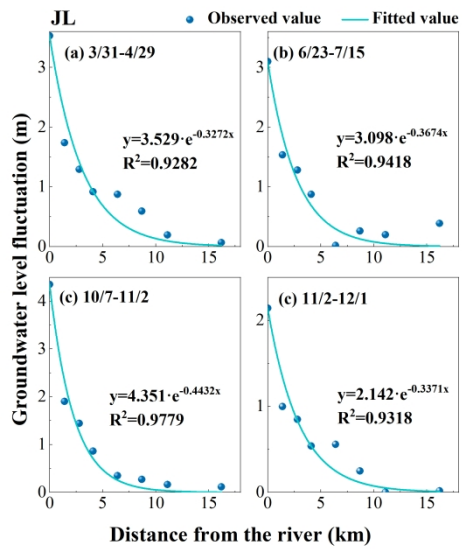
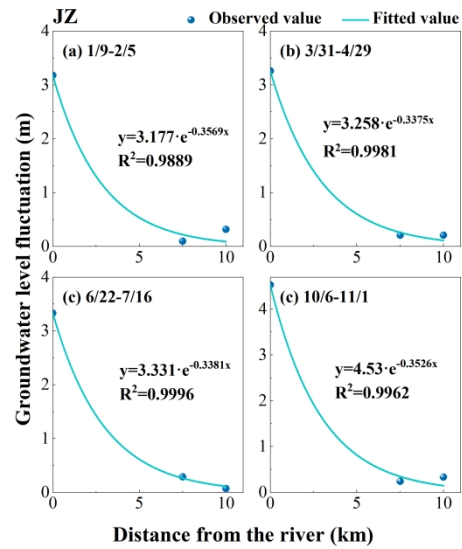
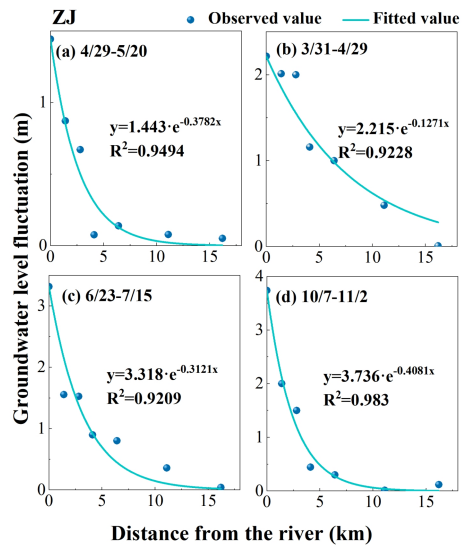


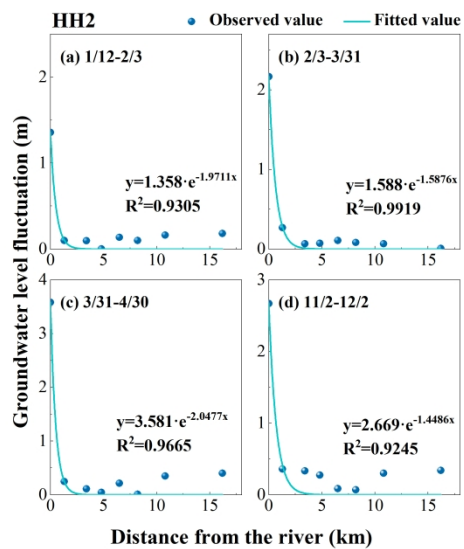
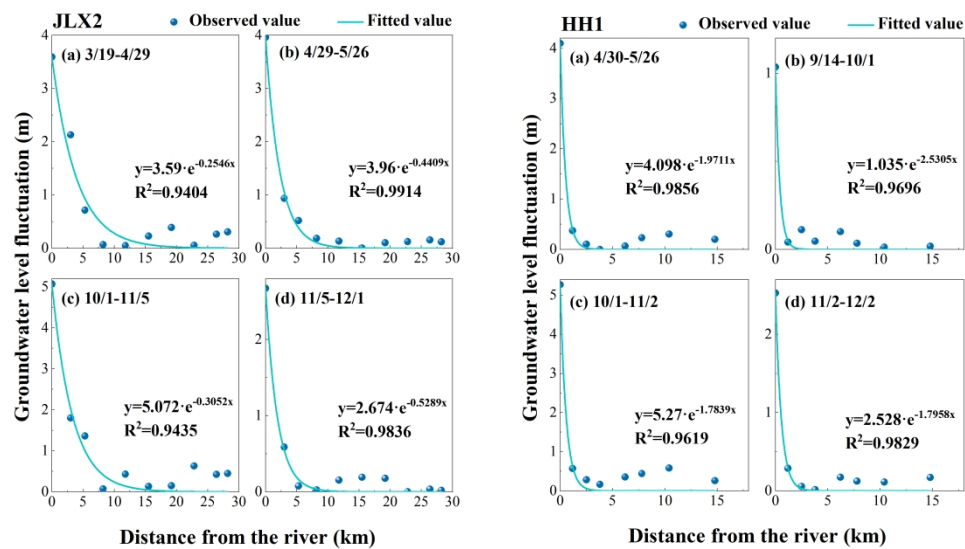


606 Figure A1. Groundwater level fluctuation y versus distance from the river x for each monitoring profile.
 607 In the legend, the A and B in "A/B" represent month and data, respectively
 608

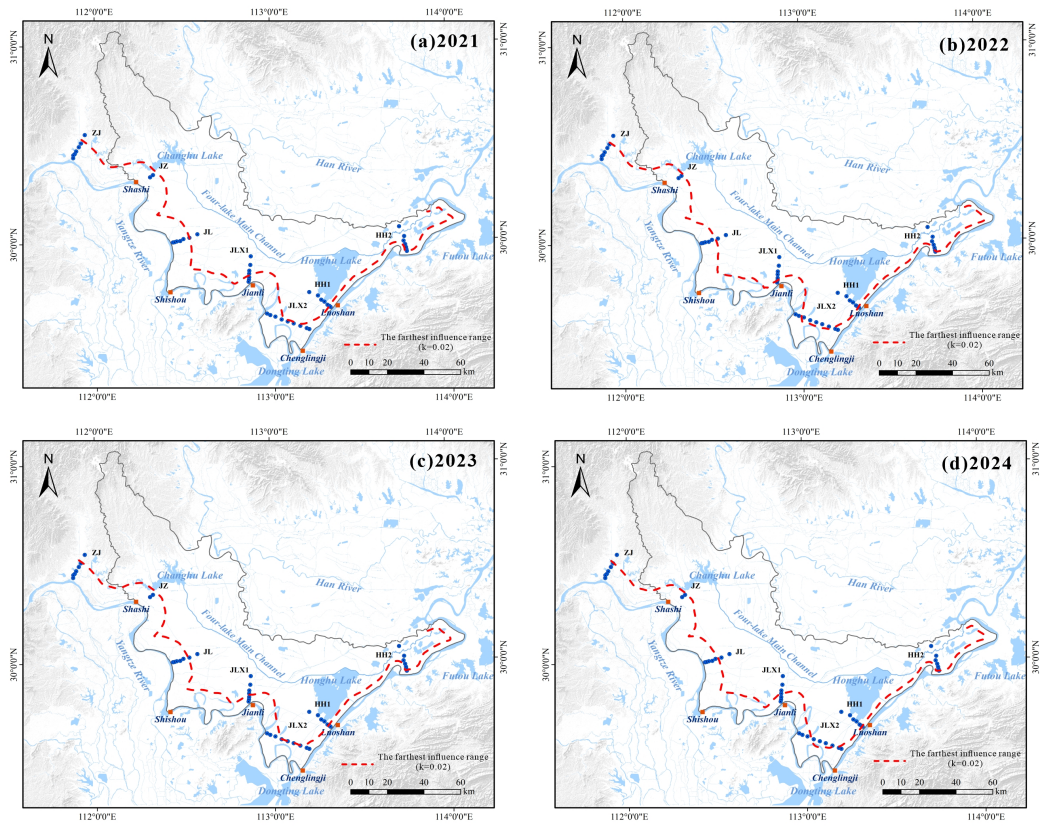


609
 610 Figure A2. Groundwater model boundary and hydrogeologic parameter zones.





611 Figure A3. The Fitting curves of groundwater level fluctuation versus distance from the river for each
 612 monitoring profile.
 613



614

615 [Figure A4. The spatial distribution of influence range of Yangtze River in four different years](#)

616

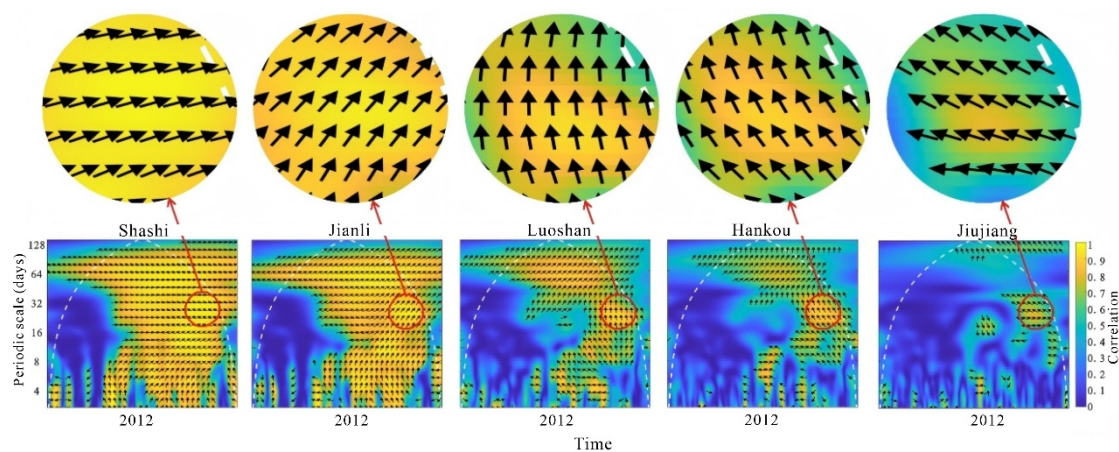
617 Wavelet coherence analysis of reservoir release and downstream river stage

618 Figure A5 is adapted from a previous study by the authors, in which continuous
 619 wavelet transform (CWT; Torrence et al., 1997) was applied to analyze the time–
 620 frequency relationship between discharge from the Three Gorges Reservoir and daily
 621 water levels at five hydrological stations along the middle Yangtze River (Shashi,
 622 Jianli, Luoshan, Hankou, and Jiujiang). The figure presents results for the year 2012
 623 as a representative example.

624 In the wavelet coherence spectra, warm colors indicate high coherence and cool
 625 colors indicate low coherence. A downstream decrease in high-coherence regions is

删除[Zhu Qi]: 4

626 evident among the five stations, with the most pronounced attenuation occurring at
627 Luoshan, suggesting a weakening influence of reservoir regulation with increasing
628 distance and tributary inflow (notably from Dongting Lake). The arrows denote phase
629 relationships between the two sets of time series data, showing a progressive increase
630 in phase lag from upstream to downstream, which indicates delayed river-stage
631 responses to reservoir discharge variations.



632
633 Figure A5. Wavelet correlation between the Three Gorges Reservoir water level and the water
634 levels at Shashi, Jianli, Luoshan, Hankou, and Jiujiang hydrological stations on the Yangtze River
635 in 2012.

删除[Zhu Qi]: 4

636

637 Code and data availability

638 Additional information regarding methodology and results is provided in the
639 Supplement.

640 Author contributions

641 Qi Zhu: conceptualization, formal analysis and writing; Ye Kang: methodology,
642 investigation and drawing; Zhang Wen: project administration and software; Hui Liu:

643 Funding acquisition and idea; Luguang Liu: monitoring work; Yan Li: field data
644 collection; Xu Li: model support, Eungyu Park: supervision and validation.

645 **Competing interests**

646 The authors declare that they have no conflict of interest.

647 **Financial support**

648 This research was partially supported by the National Natural Science
649 Foundation of China (Grant Numbers: U2340206; U23A2042; 42572313; 42272290)
650 the Natural Science Foundation of Hubei Province (2023AFD194), and the Hubei
651 Province Science and Technology Innovation Platform Project (Grant Number
652 2025CSA007).

653 **References**

- 654 Aliyari, F., Bailey, R. T., Tasdighi, A., Dozier, A., Arabi, M., Zeiler, K.: Coupled
655 SWAT-MODFLOW model for large-scale mixed agro-urban river basins,
656 *Environ. Modell. Softw.*, 115, 200–210, doi: 10.1016/j.envsoft.2019.02.014,
657 2019.
- 658 Deng, K., Yang, S., Lian, E., Li, C., Yang, C., Wei, H.: Three Gorges Dam alters the
659 Changjiang (Yangtze) river water cycle in the dry seasons: Evidence from H-O
660 isotopes, *Sci. Total Environ.*, 562, 89–97, doi: 10.1016/j.scitotenv.2016.03.213,
661 2016.
- 662 Dewey, C., Fox, P. M., Bouskill, N. J., Dwivedi, D., Nico, P., Fendorf S.: Beaver
663 dams overshadow climate extremes in controlling riparian hydrology and water
664 quality. *Nat. Commun.*, 13, 6509, doi: 10.1038/s41467-022-34022-0, 2022.

665 Du, Y., Ma, T., Deng, Y., Shen, S., Lu, Z.: Characterizing groundwater/surface-water
666 interactions in the interior of Jiangnan Plain, central China, *Hydrogeol. J.*, 26(4),
667 1047–1059, doi: 10.1007/s10040-017-1709-7, 2018.

668 Esri.: World Ocean Base [Data set]. ArcGIS Online. Retrieved from
669 [https://services.arcgisonline.com/ArcGIS/rest/services/Ocean/World_Ocean_Bas](https://services.arcgisonline.com/ArcGIS/rest/services/Ocean/World_Ocean_Base/MapServer)
670 [e/MapServer](https://services.arcgisonline.com/ArcGIS/rest/services/Ocean/World_Ocean_Base/MapServer), 2023.

671 Gao, Y., Zhang, W., Li, Y., Wu, H., Yang, N., Hui, C.: Dams shift microbial
672 community assembly and imprint nitrogen transformation along the Yangtze
673 River, *Water Res.*, 189, 116579, doi:10.1016/j.watres.2020.116579, 2021.

674 Guo, W., Zhou, H., Jiao, X., Huang, L., Wang, H.: Evaluation of hydrological regime
675 alteration and ecological effects in the middle and lower of the Yangtze River,
676 China, *Water Supply*, 22(6), 5957-5973., doi: 10.2166/ws.2022.229, 2022.

677 He B., Cai S.: The Three-Gorge Project and dynamics of shallow confined water in
678 the area of the middle reaches of the Yangtze River. *Resources and Environment*
679 *in the Yangtze Basin*, 8(1), doi: CNKI:SUN:CJLY.0.1999-01-014, 1999.

680 Hu, M., Yao, M., Wang, Y., Pan, Z., Wu, K., Jiao, X., Chen, D.: Influence of nitrogen
681 inputs, dam construction and landscape patterns on riverine nitrogen exports in
682 the Yangtze River basin during 1980–2015, *J. Hydrol.*, 617, 129109, doi:
683 10.1016/j.jhydrol.2023.129109, 2023.

684 Hu, M., Zhou, P., Chen, C.: Study on coupling of typical elements in surface water
685 and groundwater in the middle reaches of the Yangtze River, China, *J. Hydrol.*,
686 626, 130298, doi: 10.1016/j.jhydrol.2023.130298, 2023.

687 Huang, P., Zhou, A., Ma, C., Guo, J., Wang, Y., Fan, W., Li, W.: Impact of the Three
688 Gorges Dam on the spatial and temporal variation of groundwater level in
689 Jiangnan Plain using STL algorithm, *Environ. Earth Sci.*, 82(18), 417, doi:
690 10.1007/s12665-023-11110-y, 2023.

691 Huang, S., Xia, J., Zeng, S. Wang, Y., She, D.: Effect of Three Gorges Dam on
692 Poyang Lake water level at daily scale based on machine learning, *Journal of*
693 *Geographical Sciences*, 31, 1598-1614, doi: 10.1007/s11442-021-1913-1, 2021.

694 Jiang, X., Ma, R., Ma, T., Sun, Z.: Modeling the effects of water diversion projects on
695 surface water and groundwater interactions in the central Yangtze River basin,
696 *Sci. Total Environ.*, 830, 154606, doi: 10.1016/j.scitotenv.2022.154606, 2022.

697 Khaleghi, M.R., Hosseini, S.H.: Using SWAT and SWAT-CUP for hydrological
698 simulation and uncertainty analysis of the arid and semiarid watersheds (Case
699 study: Zoshk Watershed, Shandiz, Iran). *Appl. Water Sci.*, 14, 266,
700 doi:10.1007/s13201-024-02327-8, 2024

701 Lai, X., Zou, H., Jiang, J., Jia, J., Liu, Y., Wei, W.: Hydrological dynamics of the
702 Yangtze River-Dongting lake system after the construction of the three Gorges
703 dam, *Scientific Reports*, 15(1), 50, doi: 10.1038/s41598-024-83751-3, 2025.

704 Lan, Y., He, Y., Yu, Q., Song, Q.: Delineating sources of groundwater recharge in an
705 arsenic-affected aquifer in Jiangnan Plain using stable isotopes, *Hydrological*
706 *Processes*, 39, e70050, doi: 10.1002/hyp.70050, 2025.

707 Li, Y., Jing, G., Aiming, C., Jie, G., Yilin, W., Yao, Y., Youping, Z., Bo, Y.:
708 Characteristics of groundwater in the cold waterlogged paddy field of the
709 Jiangnan Plain, *Resources Environment & Engineering*, 37, 163, doi:
710 10.16536/j.cnki.issn.1671-1211.2023.02.005, 2023.

711 Liu, Y., Wang, H., Wu, Y., Zhao, Y., Ren, X.: Aquifer response to stream-stage
712 fluctuations: field tests and analytical solution for a case study of the Yangtze
713 River in Wuhan, China, *Water*, 13(17), 2388, doi: 10.3390/w13172388, 2021.

714 Maavara, T., Chen, Q., Van Meter, K., Brown, L. E., Zhang, J., Ni, J., Zarfl, C.: River
715 dam impacts on biogeochemical cycling. *Nat. Rev. Earth Env.*, 1(2), 103-116,
716 doi:10.1038/s43017-019-0019-0, 2020

717 Palmer, M., Ruhi, A.: Linkages between flow regime, biota, and ecosystem processes:
718 Implications for river restoration, *Science*, 365, 1264, doi:
719 10.1126/science.aaw2087, 2019.

720 Poff, N. L., Allan, J. D., Bain, M. B., Karr, J. R., Prestegard, K. L., Richter, B. D.,
721 Sparks, R. E., Stromberg, J. C.: The natural flow regime, *Bioscience*, 47(11),
722 769-784, doi: 10.2307/1313099, 1997.

723 Pulido-Velazquez, M., Peña-Haro, S., García-Prats, A., Mocholi-Almudever, A. F.,
724 Henriquez-Dole, L., Macian-Sorribes, H., Lopez-Nicolas, A.: Integrated
725 assessment of the impact of climate and land use changes on groundwater
726 quantity and quality in the Mancha Oriental system (Spain), *Hydrol. Earth Syst.*
727 *Sci.*, 19, 1677–1693, doi: 10.5194/hess-19-1677-2015.

728 Song, X., Chen, X., Zachara, J. M., Gomez-velez, J. D., Shuai, P., Ren, H., Hammond,
729 G. E.: dynamics control transit time distributions and biogeochemical reactions
730 in a dam-regulated river corridor, *Water Resour. Res.*, 56(9), e2019WR026470,
731 doi: 10.1029/2019WR026470.

732 Sun, Z., Huang, Q., Opp, C., Hennig, T., Marold, U.: Impacts and implications of
733 major changes caused by the Three Gorges Dam in the middle reaches of the
734 Yangtze River, China, *Water Resour. Manag.*, 26, 3367-3378, doi:
735 10.1007/s11269-012-0076-3, 2012.

736 Torrence C, Compo G P.: A Practical Guide to Wavelet Analysis, *Bulletin of the*
737 *American Meteorological Society*, 79(1), 61, 1997, doi: 10.1175/1520-
738 0477(1998)079<0061:apgtwa>2.0.co;2

739 Van Cappellen, P., Maavara, T.: Rivers in the Anthropocene: Global scale
740 modifications of riverine nutrient fluxes by damming, *Ecohydrology*, *Hydrobiol.*,
741 16(2), 106-111, doi: 10.1016/j.ecohyd.2016.04.001, 2016.

742 Wang, J., Sheng, Y., Gleason, C.J., Wada, Y.: Downstream Yangtze River levels
743 impacted by Three Gorges Dam, *Environ. Res. Lett.*, 8(4), 044012, doi:
744 10.1088/1748-9326/8/4/044012, 2013.

745 Wang, J., Wörman, A.: Spectral analysis of river resistance and aquifer diffusivity in
746 a river-confined aquifer system. *Water Resour. Res.*, 55(10), 8046–8060, doi:
747 10.1029/2018WR024639, 2019.

748 Wang, Y., Rhoads, B. L., Wang, D.. Assessment of the flow regime alterations in the
749 middle reach of the Yangtze River associated with dam construction: potential
750 ecological implications, *Hydrol. Processes*, 30(21), 3949-3966, doi:
751 10.1002/hyp.10921, 2016.

752 Wen, Z., Zhan, H., Wang, Q., Liang, X., Ma, T., Chen, C.: Well hydraulics in
753 pumping tests with exponentially decayed rates of abstraction in confined
754 aquifers, *J. Hydrol.*, 548, 40-45, doi: 10.1016/j.jhydrol.2017.02.046, 2017.

755 World Bank, 2023. Yangtze River Protection and Ecological Restoration Program
756 Program for Results (Hubei).

757 Wu, X., Wang, L., Cao, Q., Niu, Z., Dai, X.: Regional climate change and possible
758 causes over the Three Gorges Reservoir Area, *Sci. Total Environ.*, 903, 166263,
759 doi: 10.1016/j.scitotenv.2023.166263, 2023.

760 Xie, Y., Tang, Y., Chen, X., Li, F., Deng, Z.: The impact of Three Gorges Dam on the
761 downstream eco-hydrological environment and vegetation distribution of East
762 Dongting Lake, *Ecohydrology*, 8(4), 738-746, doi: 10.1002/eco.1543, 2014.

763 Xiong, J., Yin, J., Kyaw Tha Paw U, Zhao, S., Qiu, G., Liu, Z.: How the three Gorges
764 Dam affects the hydrological cycle in the mid-lower Yangtze River: a

765 perspective based on decadal water temperature changes, *Environ. Res. Lett.*, 15,
766 014002, doi: 10.1088/1748-9326/ab5d9a, 2020.

767 Yang, Y., Yuan, Y., Xiong, G., Yin, Z., Guo, Y., Song, J., Zhu, X., Wu, J., Wang, J.,
768 Wu, J.: Patterns of nitrate load variability under surface water-groundwater
769 interactions in agriculturally intensive valley watersheds, *Water Res.*, 267,
770 122474, doi: 10.1016/j.watres.2024.122474, 2024.

771 Yang, S., Milliman, J. D., Xu, K., Deng, B., Zhang, X., Luo, X.: Downstream
772 sedimentary and geomorphic impacts of the Three Gorges Dam on the Yangtze
773 River, *Earth-Sci. Rev.*, 138, 469-486, doi: 10.1016/j.earscirev.2014.07.006, 2014.

774 Yang, S., Zhang, J., Xu, X.: Influence of the Three Gorges Dam on downstream
775 delivery of sediment and its environmental implications, *Yangtze River*,
776 *Geophys. Res. Lett.*, 34(10), doi: 10.1029/2007GL029472, 2007.

777 Zhang, Q., Li, L., Wang, Y., Werner, A., Xin, P., Jiang, T., Barry, D.: Has the Three-
778 Gorges Dam made the Poyang Lake wetlands wetter and drier? *Geophys. Res.*
779 *Lett.*, 39(20), 28, doi: 10.1029/2012GL053431, 2012.

780 Zhang, S., Zhai, X., Yang, P., Xia, J., Hu, S., Zhou, L., Fu, C.: Ecological health
781 analysis of wetlands in the middle reaches of Yangtze River under changing
782 environment, *Int. J. Digit. Earth*, 16(1), 3125–3144, doi:
783 10.1080/17538947.2023.2244471, 2023.

784 Zhou, M., Xia, J., Deng, S., Shen, J., Mao, Y.: Modelling of phosphorus and
785 nonuniform sediment transport in the Middle Yangtze River with the effects of
786 channel erosion, tributary confluence and anthropogenic emission. *Water Res.*,
787 243, 120304, doi: 10.1016/j.watres.2023.120304, 2023.

788 Zhou, Y., Wang, Y., Li, Y., Zwahlen, F., Boillat, J.: Hydrogeochemical characteristics
789 of central Jiangnan Plain, China. *Environ. Earth Sci.*, 68(3), 765–778, doi:
790 10.1007/s12665-012-1778-9, 2013.

